National Institute of Laser Enhanced Sciences, JLSA's Vol.01. Issue.1 (2024) 10-20

NILES

Journal of Laser Science and Applications
journal homepage: https://jlsa.journals.ekb.eg

Cairo University

A High Sensitive Refractive Index-Based Terahertz Biosensor for Virus Detection

Zienab EL-Wasif[1], Omnia Hamdy[1*], and Tawfik Ismail[1,2]

[1]National Institute of Laser Enhanced Sciences, Cairo University, Giza 12613, Egypt
[2]College of Engineering, Taibah University, Madinah 42353, Saudi Arabia

Abstract

Purpose: To design and analyze a highly sensitive and stable metamaterial-based Terahertz (THz) biosensor for virus detection.
Methods: The proposed THz biosensor utilizes a flower-shaped resonator design enabling miniaturization and precise control over THz pulse interaction with biological samples. The sensor's design is characterized, and its sensitivity is evaluated based on refractive index measurements. The analysis includes assessing the sensor's performance against different viruses including M13 bacteriophage, HSV, Influenza A, and HIV-1. The influence of sample thickness is also examined. The implementation involves determining the peak theoretical sensitivity and estimating the sensor's free space absorptivity.
Results: The biosensor has a footprint of 0.751 λeff × 0.751 λeff, where λeff represents the wavelength at the operating frequency 8.0299 THz. The sensor demonstrates a peak theoretical sensitivity of 924 GHz/Refractive Index Unit (RIU) with an estimated absorptivity of 99.9% in free space. The sensor's rotational symmetry ensures polarization insensitivity, stability up to 90° of incident angle and insensitivity to incident modes. The performance evaluation against multiple viruses reveals an average sensitivity of 891.917 GHz (RIU) and a high Figure of Merit.
Conclusion: The results demonstrate its potential for detecting viruses such as M13 bacteriophage, HSV, Influenza A, and HIV-1. The proposed sensor contributes to advancing virus detection methods.

Keywords— THz Sensors; Metamaterials; Biomedical Sensors; Viruses.

I. Introduction

The non-ionizing and non-injurious characteristics of Terahertz (THz) radiation have captivated researchers, making it a compelling choice for various biomedical applications. The electromagnetic spectrum within the range of 0.1 to 10 THz has found wide utility in biomedical sensing, imaging, and spectroscopy. This frequency range offers enhanced surface penetration capabilities while keeping energy consumption to a minimum. Moreover, THz radiation exhibits reduced harmful effects, rendering it suitable for disease diagnosis purposes. Consequently, THz radiation has been extensively investigated across scientific disciplines, including sensing [1-5], spectroscopy [6], imaging [7-9], material characterization [10], and communication [11]. Its versatile nature has paved the way for diverse research endeavors in these fields.

THz radiation is frequently utilized in biosensing technology to analyze biological samples in a non-invasive mode. It is generated using methods like quantum cascade lasers and photoconductive switches [12, 13]. The purpose of biosensors is to improve the interaction between THz radiations and samples so that structural properties and molecular vibrations may be studied. To turn THz signals into quantifiable data, detection techniques including bolometers and photoconductive antennas are employed. Applications in molecular imaging, material characterization, and medical diagnostics are made possible by the integration of THz radiation generation, sensor manipulation, and detection. For label-free biosensing, THz radiation offers special benefits [14, 15].

In recent years, there has been a widespread adoption of metamaterials in the development of miniaturized THz structures and devices. Metamaterials are artificially engineered materials with adjustable permittivity, permeability, and refractive index characteristics [16]. This unique property has facilitated the creation of resonant components with low loss such as sensors and absorbers, enabling their utilization in diverse applications including material analysis and biomedical sensing. The controllability of the electromagnetic properties of metamaterials has opened up new avenues for precise manipulation of THz waves leading to enhanced performance and functionality in THz-based systems. The integration of metamaterials has significantly contributed to advancements in THz technology and expanded its potential in various scientific and technological domains.

The fundamental idea revolves around the development of a dedicated THz sensor tailored for the detection of viruses. This sensor is engineered to undergo changes in its

Received 5-17-2024 accepted 6-12-2024
Corresponding author: Omnia Hamdy Email: omnia@niles.cu.edu.eg

resonant properties when it interacts with THz radiation in the presence of a virus sample. Parameters such as transmission, reflection, and absorption coefficients are affected by the presence of the sample. Among these parameters, the performance evaluation of the proposed sensor primarily focuses on its absorptivity. By analyzing the sensor's absorptive behavior, researchers can gain insights into its sensitivity and effectiveness in virus detection, thus highlighting its potential for practical applications in the field.

THz metamaterial absorbers have gained significant traction in the literature, particularly in the realm of material characterization. In a notable study [17], researchers successfully developed an ultrasensitive metamaterial THz star-shape biosensor with an absorption rate of 97.2%. The sensor was specifically designed for the detection of coronaviruses and other flu viruses. The proposed sensor had a footprint of $0.609_{\lambda eff} \times 0.609_{\lambda eff}$, where λ_{eff} is the wavelength determined at the operating frequency of 1.9656 THz. The full-width at half-maximum (FWHM) is 5.276% compared to absorption frequency with a Q-Factor of 19.08.

In another study, Veeraselvam et. al. [18] developed a highly sensitive metamaterial sensor having an absorption rate of 99.9%. Their proposed miniaturized THz sensor employed a fan-shaped resonator enclosed within a square loop, yielding a compact footprint measuring 0.353λeff × 0.353λeff. Here, λeff represented the wavelength calculated at the operating frequency of 4.87 THz. These developments highlight the growing utilization of metamaterial-based THz sensors for precise and efficient detection of biological samples and viral pathogens.

Anchen et al. [19] introduced a novel and highly effective approach by proposing a centrosymmetric double F-shaped metal resonator with an absorption rate of 95%. This ultra-sensitive metamaterial design exhibited a size of 1.029λeff × 1.209λeff, (λ_{eff} is the wavelength calculated at the operating frequency of 5.92 THz). This resonator demonstrated a remarkable Q factor of 49.6, indicating its ability to sustain high-quality resonances and efficient energy transfer. In their study, Keshavarz et al. [20] investigated a nanoscale metamaterial reflector utilizing Fano-resonances. The design incorporated a graphene H-shaped antenna positioned at the center of an InSb semiconductor film. Through numerical analysis, the researchers demonstrated that the proposed nano-biosensor served as an effective sensing platform for the detection of Avian Influenza (AI) viruses, including H1N1, H5N2, and H9N2. These viruses exhibited distinct complex values of the refractive indexes (RI). The nano biosensor achieved a maximum sensitivity of 540 GHz/RIU (Refractive Index Unit), highlighting its remarkable capability to detect subtle changes in the RI of the target viruses.

Dong Cheng et al. [21] successfully developed a metamaterial absorber utilizing Jerusalem cross apertures. This absorber relied on the excitation of strongly confined spoof surface plasmon polariton resonance modes in the THz regime. The researchers focused on biosensing different subtypes and protein concentrations of Avian Influenza (AI) viruses, specifically H5N2, H1N1, and H9N2. Each subtype virus exhibited a distinct frequency deviation: 0.36 THz, 0.36 THz, and 0.51 THz, respectively.

This work designs and analyses a miniaturized THz metamaterial biosensor with exceptional sensitivity. The proposed miniature metamaterial building block is a subwavelength component employed in forming an almost limitless regular arrangement. The sensor was constructed utilizing a star-shaped resonator. The estimated peak absorptivity is 99.9% worked at an operating frequency of 8.0299 THz for the proposed THz metamaterial biosensor with a Q-factor (Q) and full-width half maximum (FWHM) greater than 33 and 242 respectively. To assess the sensing capability of the proposed sensor with maximum sensitivity more than 920 GHz/RIU, theoretical values of the refractive index of several viruses, such as HSV, Influenza A, HIV-1, and M13 bacteriophage, are used. It continues to function efficiently even with a ±5% fabrication tolerance and is stable at angles of up to 90°. Following the introduction section, the remainder of the manuscript is structured as follows: in section 2, the design and characterization of the proposed biosensor are presented. Section 3 examines the polarization and angular stability, while section 4 provides an in-depth analysis of the biosensor's sensitivity. The design and analysis of the THz metamaterial biosensor were carried out using CST Studio Suite 2024.

II. BIOSENSOR DESIGN

A. *Sensor's Construction*

Figure 1 shows the geometry and dimensions of the THz metamaterial biosensor under discussion. **Figure 1(a)** highlights the sensor's specific dimensions, while **Figures 1(b) and 1(c)** show its side and perceptive views. The biological sensor with a footprint of 15 (L) µm x 15 (L) µm is designed to reach the best absorption peak [22]. A parameter sweep was carried out in CST Microwave Studio to fine-tune the biosensor design and attain the maximum absorption peak. The parameter sweep enables users to investigate different aspects of the biosensor and assess their impact on the absorption properties.

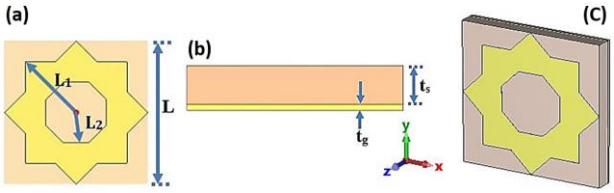

Figure 1: Unit cell of the proposed THz sensor: L_1= 7.5 µm and L_2= 4.5 µm with thickness $\Delta L = L_1 - L_2$ = 3 µm and upper gold has a thickness of 3 nm, t_g = 0.25 µm , t_s=1.6 µm, (a) Top view (b) Side view (c) Perspective view

Incorporating a figure on an ultra-thin lossy polyimide substrate improves sensor performance substantially. The substrate exhibits permittivity 3.5, loss tangent 0.0027 [23], and thickness ts = 1.6 µm. The substrate is positioned between the gold top and bottom conductors. The Gold layer is modelled as a lossy medium with a frequency-independent conductivity of 4.09 × 107 S/m [22, 23]. In terms of sensor architecture, the top portion has a frequency-selective flower-shaped geometry, as shown in **Figure 1(a).** The bottom section has a 0.25 µm thick gold conductive ground layer (tg

= 0.25 μm). The suggested metamaterial absorber has geometrical parameters: L1 = 7.5 μm, L2 = 4.5 μm, and ΔL = L1 - L2 = 3 μm. Figs. 1(a) and (b) show that the upper layer of gold is 3 nm thick. This also results in a large FWHM which further impacts the Figure of Merit (FoM).

B. Simulation

For simulation, we utilized a FIT numerical simulation program CST Microwave Studio 2024. In the frequency domain solver of the full-wave EM solver CST Microwave Studio, the accuracy is achieved by setting the number of mesh lines per wavelength to 15 and the accuracy to 10-6. Additionally, periodic boundary conditions are applied in the X and Y directions for the TE and TM modes, along with electric and magnetic boundaries in the X and Y directions for the TEM mode, and open boundaries in the Z-direction. The optimal absorber characteristic is achieved by maximizing the absorption coefficient (A), which can be computed as follows [25, 26]:

$$A(\omega) = 1 - |S11|^2 - |S21|^2 \quad (1)$$

where S11 and S21 depict the reflection and the transmission coefficients respectively. In our work, the absence of transmission (S21 = 0) is attributed to the presence of the bottom gold layer serving as a ground plane as illustrated in **Figure 2**. Transverse electric magnetic (TEM) polarized waves that incident ordinarily on air serve as the first source of excitation for the proposed structure. **Figure 2** shows the reaction in terms of absorption, reflection, and transmission. The peak absorptivity is recorded at 99.9% and zero reflection at an operating frequency of 8.0299 THz. To assure accuracy in the frequency domain solver of the full-wave EM solver CST Microwave Studio, the following parameters were used: the number of mesh lines per wavelength was set to 15, and the desired precision was set to 10-6. For the TE and TM modes, periodic boundary conditions were imposed in the X and Y directions, while the TEM mode had electric and magnetic boundaries in the X and Y directions. Open boundaries were used in the Z-direction to allow for proper wave propagation.

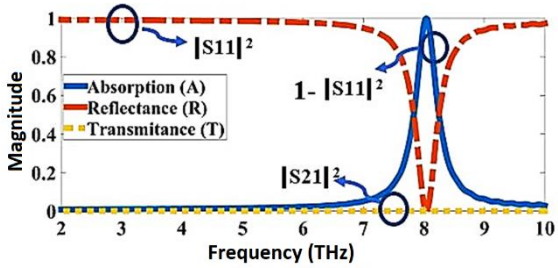

Figure 2: Absorption, Reflection, and Transmittance characteristics of the proposed THz sensor for TEM.

The absorption mechanism can be elucidated by computing the relative impedance, which is provided by (18, 20):

$$Z(\omega) = \sqrt{\frac{(1+S_{11})^2 - S_{21}^2}{(1-S_{11})^2 - S_{21}^2}} \quad (2)$$

The metallic cube inhibits backward propagation, resulting in S21 = 0; therefore, the impedance can be defined as:

$$Z(\omega) = \frac{(1+S_{11})}{(1-S_{11})} \quad (3)$$

Moreover, utilizing (3), absorbance can be alternatively represented as:

$$A(\omega) = \frac{4\mathrm{Re}(Z)}{(1+\mathrm{Re}(Z))^2 + (\mathrm{Im}(Z))^2} \quad (4)$$

Equation (4) suggests that unity absorption occurs when the real part of the impedance Re(Z) approaches unity, and the imaginary part, Im(Z), approaches zero, as depicted in **Figure 3 (a)** at resonance frequency 8.0299 THz. The surface current density, the magnitude electric field, and the magnitude magnetic field distribution are also presented in **Figure.3 (b), (c),** and **(d)**, respectively. As presented in the figure, the field is well confined to the edges of metal which leads to a high absorptivity of 99.9% at an operating frequency of 8.0299 THz.

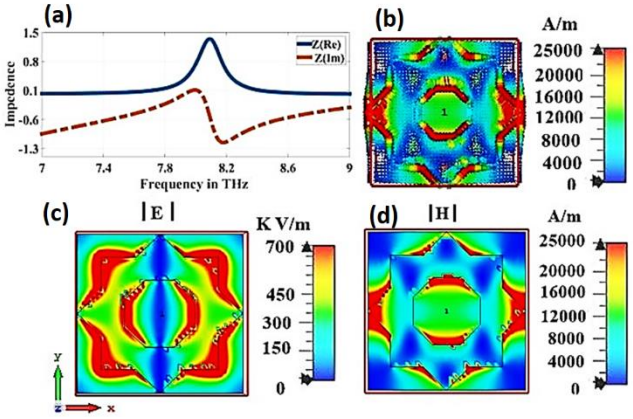

Figure 3 (a) Effective impedance, (b) surface plasmon density, (c) Magnitude electric field distribution, and (d) Magnitude Magnetic field distribution characteristics of the proposed THz sensor

C. The evolution of the proposed design of sensor

Figure 4 illustrates the development of the proposed THz biosensor, showcasing its key components. In particular, **Figure 4(a)** showcases a square resonator, while **Figure 4(b)** highlights a rhombus resonator that is formed at the center of the square substrate. These resonators play a crucial role in the functionality of the THz sensor. Additionally, **Figure 5** presents the absorption properties associated with the proposed THz biosensor. It provides insights into how the sensor interacts with THz radiation, thereby enabling the detection and analysis of relevant biological samples. The square with thickness $\Delta L = L_1 - L_2 = 3$ μm is equal to the thickness of the rhombus. The square resonator works at 5.57 THz and obtains 74.4% at. The diamond resonator operates at 8.75 THz and offers 81.5% absorptivity as depicted in **Figure.5**. The proposed flower shape is formed by synthesizing a square resonator and a rhombus resonator to achieve 99.9% at 8.0299 THz.as shown in **Figure 4 (c)** and **Figure 5**.

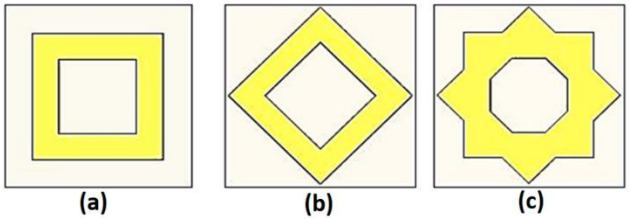

Figure 4: The gradual development of the suggested THz sensor design, (a) The first resonator, (b) the second resonator, (c) the proposed Resonator.

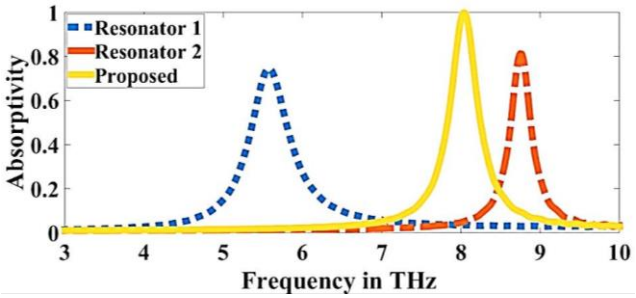

Figure 5: Absorption features during different phases of evolution.

III. Stability Analysis

This section evaluates and discusses the suggested THz sensor's polarization and angular stability. THz radiation is directed towards the direction of the 'Z' on the sensor. Under normal incidence ($\theta = 0^o$), polarization stability is investigated for both transverse electric (TE) and transverse magnetic (TM) modes with $\phi = 0^o$ and $\phi = 90^o$, respectively. As shown in **Figure 6(a)**, the proposed THz sensor's rotational design produces equal absorption characteristics for both the TE and TM modes, reaching 99.4% at 7.86 THz. The sensor exhibits insensitivity to incident polarized THz waves, regardless of their polarization. Furthermore, THz waves at oblique incidence and their effects on absorption properties are studied and illustrated in **Figure 6(b).**

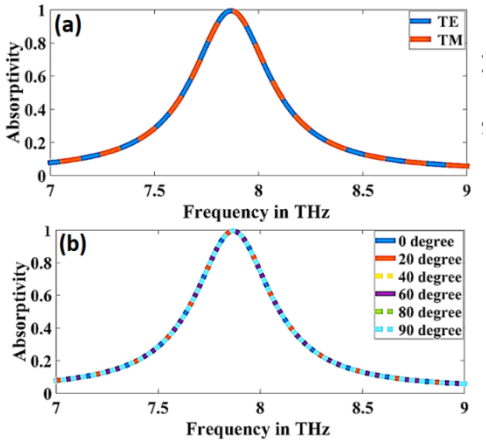

Figure 6 Polarization stability and (b) Features of the suggested sensor's angular stability.

A sensor's angular stability is defined as the range of angles (θ) where it exhibits constant characteristics without any frequency fluctuation or absorption degradation. As a result, the suggested THz sensor demonstrates angular independence up to $\theta = 90^o$. The sensor responds to oblique incidence in the same way in both the TE and TM modes because of its polarization-independent construction. Therefore, compared to previous research [22, 25], it can be concluded that the suggested sensor is impervious to polarization and exhibits perfect angular independence. According to El-Wasif et al. [25], angular stability is defined as having similar countenances with an absorptivity of more than 95% and a frequency deviation of less than 0.05 THz. Similar parameters were estimated for angular stability in [22], with frequency deviation less than 0.1 THz and absorptivity greater than 80%. This characteristic makes the suggested structure appropriate for fast detection.

IV. Sensitivity Estimation

A. *Effect of materials*

The proposed sensor's performance is assessed by varying the thickness of the sample and the sample material's refractive index profiles as depicted in **Figure 7** and **Figure 8**. The quality factor (Q) serves as a crucial metric for evaluating sensor performance, relying on parameters such as resonant frequency (fr) and full-width half maximum (FWHM), as described by [22, 25]:

$$\boldsymbol{Q} = \frac{\mathbf{fr}}{\mathbf{FWHM}} \tag{5}$$

The sensor is subjected to analytes with different thicknesses and refractive indices in order to analyze the sensing performance of the proposed sensor. The capacitance that the analyte under investigation induces, known as sensing capacitance (Csensor), and the device capacitance (arising from the dielectric between the two metal layers) are both necessary for the sensor's effective capacitance (Ceff) [22, 24]. Consequently, alterations in the refractive index of the analyte lead to changes in the sensing capacitance (Csensor), thereby affecting the effective capacitance (Ceff) of the metamaterial sensor. This alteration in effective capacitance affects the $\boldsymbol{Q}$ of the sensor, expressed as $\boldsymbol{Q} = 1/\boldsymbol{\omega_{CR}}$. In the present study, an increase in refractive index elevates the effective capacitance, consequently reducing the Q factor. Thus, the resonant frequency of the metamaterial sensor decreases as a result of this decrease in Q factor clarifying the basic physics behind the functioning of the suggested metamaterial sensor.

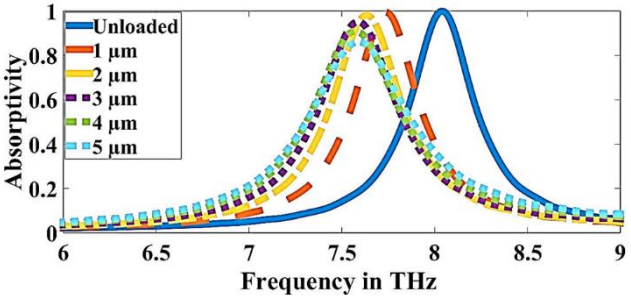

Figure 7: Absorption characteristics for various the thickness of analyte.

The sensor's performance is assessed for a range of sample thicknesses based on **Figure 7**. We take into account the refractive index n = 1.5 for varying sample thicknesses. When the biological analyte with a thickness of 1 µm is placed onto the suggested THz sensor, a red shift of 297 GHz is seen. In the case when the analyte thickness is changed from 1 to 5 µm, the estimated average frequency variation is 411.24 GHz/µm. As the sample's refractive index is changed for a sample thickness of 3 µm, **Figure 8** shows the matching absorption properties. The figure's analysis shows that absorptivity decreases as refractive index values rise. The expression for sensitivity (S) is [22, 25]:

$$\mathbf{S} = \frac{\mathbf{\Delta f}}{\mathbf{\Delta n}} \qquad (6)$$

where Δf is the ratio of frequency deviation and Δn is the change in refractive index. The analysis shows that the suggested sensor provides an average sensitivity of more than 848 GHz/RIU for refractive indices between 1.1 and 1.6. Accordingly, the suggested THz sensor shows great sensitivity to refractive index variations in the sample material with absorptivity surpassing 93% and a maximum sensitivity of 924 GHz/RIU for refractive index variations up to 1.6 (see **Figure 8 (b)**). With changing refractive indices, Table.1 provides a detailed description of the absorptivity A, sensitivity S, resonance frequency Fr, and frequency deviation Δf.

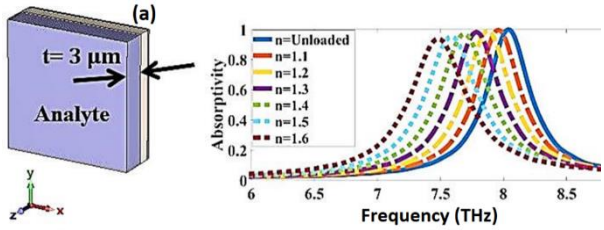

Figure 8: A setup for experiments that estimates sensor performance for sensitivity in a variety of materials with different indices of refraction.

Table 1 The frequency shift and sensitivity of different refractive indices.

RI	A%	Fr (THz)	Δf (GHz)	S, (GHz/RIU)
1	99.9	8.0299	-	-
1.1	99.65	7.9507	79.2	792
1.2	99.1	7.8715	158.4	792
1.3	98.185	7.7824	247.5	825
1.4	96.91	7.6834	346.5	866.25
1.5	95.25	7.5844	445.5	891
1.6	93.25	7.4755	554.4	924

Figure 9 illustrates the impact of dispersion on absorption characteristics at a refractive index of 1.3. Analyzing dispersion necessitates consideration of the loss tangent [22, 25] which is estimated at the operational frequency. To examine absorption characteristics, the loss tangent varied from 0.0057 to 0.28, and the results are depicted in **Figure 9**.

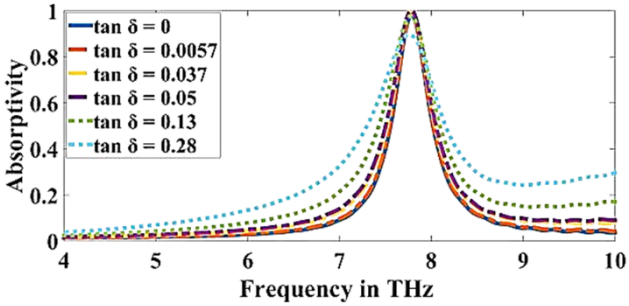

Figure 9: Effect of dispersion on the proposed sensor for refractive index 1.3

The graph shows that the suggested THz sensor's frequency does not change as a result of the sample's dispersion properties. Despite the sample's inherent loss, absorption characteristics decrease. Nevertheless, a minimum of 89.71% absorption is ensured across the range of 0.0057–0.28. In [25], Values ranging from 0.0057 to 0.28 guarantee a minimum of 66% absorption at the low resonance frequency (1.9656 THz) and 43.9% absorption at the high resonance frequency (3.3692 THz). In [22] the samples have a high loss rate results in a reduction of absorption characteristics. Nonetheless, a minimum absorption of 50% is assured for values between 0.0057 and 0.28.

B. Impact of biomedical samples

The increasing trend in biophotonics and biomedical applications towards better, more affordable, and compact systems. It also mentions the close relationship between biophotonics and developments in THz biosensors and detectors for sensing biomarkers based on changes in refractive index. It mentions an investigation into the detection of four viruses with different refractive indices. The viruses that were used in this research were discussed in detail as follows:

1. HSV Virus: The Herpes simplex virus (HSV) belongs to the Herpesviridae family and is categorized as a DNA virus with two serotypes: HSV-1 and HSV-2. HSV-1 commonly affects the oral and ocular regions, while HSV-2 predominantly causes genital tract manifestations [27-29]. Both serotypes affect a significant portion of the global population and pose risks to immunocompromised individuals. HSV transmission occurs through direct contact, leading to lifelong latent infection in neural cells with potential reactivation under immunocompromised conditions. Diagnosis relies on laboratory confirmation due to limitations in clinical presentation accuracy. Common diagnostic methods include viral antigen detection, virus culture, molecular biology, and cytological examination [30-32].
2. Influenza A Virus: The Influenza virus highlights its RNA nature and classification into types A, B, and C [33]. It discusses the common manifestation of the virus in the upper respiratory tract, leading to acute viral infections with the potential for severe complications [34, 35]. Influenza types A and B are responsible for seasonal epidemics, with type A having the ability to cause sporadic pandemics due to

antigenic variation [36, 37]. Diagnosis based solely on clinical symptoms is not accurate, necessitating laboratory studies for appropriate therapeutic approaches. Various diagnostic methods, including conventional, serological, and molecular techniques, are available for diagnosing Influenza [38].

3. HIV Virus: Human Immunodeficiency Virus (HIV), detailing its classification as an RNA virus belonging to the Retroviridae family [39]. It explains how HIV causes acquired immunodeficiency syndrome (AIDS) by weakening the immune system and affecting multiple bodily systems [39, 40]. Global statistics on HIV prevalence and transmission methods are mentioned, emphasizing the direct exchange of bodily fluids as the primary mode of transmission. In addition, the significance of HIV testing, recommending universal testing for individuals aged 13 to 64 [41]. Diagnostic methods such as ELISA, Western blot, PCR, and rapid antigen/antibody tests are discussed, with attention to their limitations, particularly in diagnosing infants and recently infected patients. Overall, the passage highlights the importance of HIV awareness, testing, and diagnostic strategies in combating the spread of the virus and managing its impact on public health [42].
4. M13 Bacteriophage: Bacteriophages (or bacterial viruses) highlight their classification as genetic elements within prokaryotic cells [43]. Bacteriophages are found in diverse environments globally and play roles that include modulating bacterial populations through mechanisms such as killing host bacteria, gene transfer, and competition mediation [44]. Advancements in electron microscopy have enabled detailed study and diagnosis of bacteriophages, with techniques such as cryoelectron microscopy, three-dimensional image reconstruction, particle counting, immunoelectron microscopy, and transmission electron microscopy being utilized [45]. The significance of bacteriophages in microbial ecosystems reveals the importance of advanced microscopy techniques in understanding their biology and functions [46].

Figure 10 presents the four studied viruses (HSV, Influenza A, HIV-1, and M13 bacteriophage viruses) with RI of 1.41, 1.48, 1.5, and 1.57 [47]. The close values of viruses' refractive indices typically indicate underlying similarities in their physical structure, chemical composition, and genetic makeup, providing insights into their interactions and behaviors. The frequency shifts from 7.6735 THz to 7.5052 THz when the RI is changed from 1.41 (HSV virus) to 1.57 (M13 bacteriophage). Viruses can be sensed because of changes in the absorption peak position caused by variations in the virus's RI which is used for detection. A detailed plot showing frequency deviation and absorptivity fluctuation is shown in **Figure 10(a)**. The sensitivity of the suggested THz biosensor was also established and shown in **Figure 10(b)**. The maximal sensitivity is approximately 920 GHz/ RIU, as shown in Fig. 10(b) which is a great value for virus detection devices.

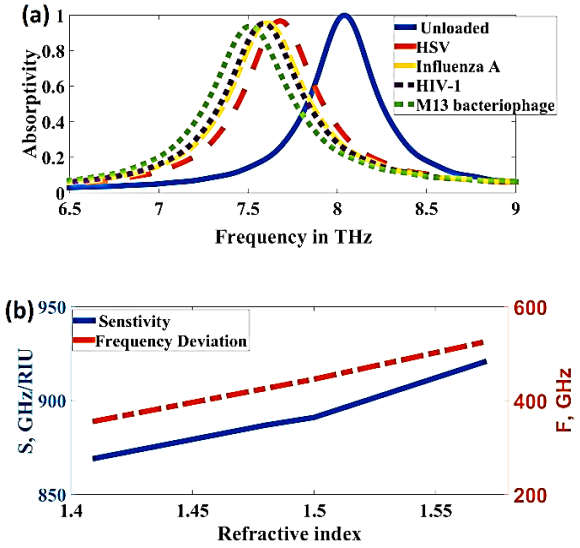

Figure 10(a) Sensor performance for difference viruses based on refractive index change, (b) Frequency deviation and sensitivity performance for difference viruses.

Table.2 outlines the sensor metrics for the flower-shaped THz refractive index sensor proposed. Notably, the proposed THz sensor exhibits high sensitivity at n = 1.57, registering 920 GHz/RIU, whereas a lower sensitivity of 869.2 GHz/RIU is observed at $n = 1.41$. Parameters such as frequency deviation (Δf), Full-Width Half Maximum (FWHM), Q-factor, and Figure of Merit (FoM) are calculated and displayed in **Table 2.** Across various viruses, the frequency deviation surpasses 356.4 GHz while the FWHM remains below 250.19 GHz. With a refractive index ranging from 1.41 to 1.57, the suggested biosensor shows an average Q factor of 30.85. For the M13 bacteriophage ($n = 1.57$), the peak value is 3.827, indicating that the FoM is expected to be more than 3.47. As stated in [22, 25], the FoM is:

$$\boldsymbol{FoM = \frac{S}{FWHM}} \tag{7}$$

Table 2 Absorption properties of HSV, Influenza A, HIV-1, and M13 bacteriophage viruses for different refractive indices.

Type of viruses	RI	A%	Fr THz	Δf (GHz)	FWHM (GHz)	Q-Factor	S, (GHz/RIU)	FoM
Unloaded	1	99.9	8.0299	-	242.05	33.1745	-	-
HSV	1.41	96.783	7.6735	356.4	250.19	30.67	869.268	3.4744
Influenza A	1.48	95.622	7.6042	425.7	247.63	30.7	886.875	3.58145
HIV-1	1.5	95.254	7.5844	445.5	245.94	30.83	891	3.62283
M13 bacteriophage	1.57	93.8899	7.5052	524.7	240.53	31.2027	920.526	3.82707

Table 3 Fabrication tolerance study for ΔL and the upper 3-nm gold layer

Parameter	Tolerance	Fr THz	Δf (GHz)	%Deviation	Absorption for n=1
ΔL	%5-	8.0596	29.7	3.698	99.72
	%5+	8.0002	29.7	3.698	99.95
The upper Nanolayer	%5-	8.0229	0	0	99.916
	%5+	8.0229	0	0	99.922

Table 4 Comparing the FoM, Q-factor, and sensitivity across various research studies.

Ref.	Dimension of the structure μm × μm	Ns	t μm	Fr THz	FWHM (GHz)	S, (GHz/RIU)	Q	FoM (RIU)-1
(48)	80 × 80	1.6	-	0.85	-	182	-	-
(49)	50 × 50	1.6	11	1.67	400	455.7	-	-
(50)	120 × 120	1.8	8	0.81	-	240	3.45	-
(23)	80 × 80	1.33	-	1.85	140	423	13.2	3.02
(51)	54 × 70	1.6	18	1.94	300	550	6.46	1.8333
(25)	64.15 × 64.15	1.6	10	1.9656	90.531	836.333	21.71	9.238
This Work	15 × 15	1.6	3	8.0229	242.05	924	30	3.686

Regarding the ultra-thin lossy polyimide substrate, **Table 3** illustrates the fabrication errors within ±5% during conductor deposition. To determine the fabrication tolerance, three factors are taken into consideration: the width of the square, the width of the flower-shaped resonator thickness, and a rhombus, represented by $\Delta L = L_1 - L_2$. By offering absorptivity greater than 98% for n = 1, the results show that the suggested biosensor can tolerate fabrication faults. The estimated frequency deviation is 29.7 GHz with deviation of less than 4% for every change in ΔL of the proposed sensor. The proposed sensor is more stable than [22] with no degradation in the absorption peak and no shift in deviation as the upper gold nanolayer thickness changes. In contrast, [22] reported absorption of higher than 98% and a frequency deviation of more than 570 GHz with a deviation rate > 11% for each increase in the upper gold nanolayer thickness.

A detailed performance comparison of the suggested biosensor with other sensors reported in the literature is given in **Table 4.** Based on information from pertinent literature sources, this comparison is made using the analyte's thickness and refractive index. When compared to the references, the suggested sensor is the most compact, according to the table analysis. [23, 25, 48–51].

In summary, our proposed biosensor provides the following features:

- The proposed sensor exhibits exceptional peak absorption of 99.9% at a frequency of 8.0299 THz. This indicates the sensor's remarkable ability to efficiently capture and interact with THz radiation at this specific frequency making it highly suitable for various applications requiring high absorption capabilities.
- The average sensitivity of the proposed sensor is measured to be 848.375 GHz/RIU at a frequency of 4.87 THz. This sensitivity value surpasses the sensitivities reported in previous studies [23,25, 48–51]. This indicates its enhanced capability to detect and measure changes in refractive index units (RIU).
- The operational characteristics of the proposed sensor demonstrate a commendable level of stability across various sample thicknesses. The average deviation observed in these operational characteristics is 350.74 GHz/μm. This indicates that the sensor's performance remains consistent and reliable even when different sample thicknesses are considered.
- The proposed sensor achieves an improved FWHM of 242.05 GHz, accompanied by a quality factor of 33.1745. This narrower FWHM indicates a higher resolution and sensitivity in detecting subtle changes in the refractive index. Furthermore, the obtained FoM exceeds 3 indicating the sensor's enhanced performance and suitability for detecting various refractive index profiles associated with different viruses.
- A better loss of tangent Absorption characteristics decreases than [22, 25] as we mentioned earlier because a minimum of 89.71% absorption is ensured across the range of 0.0057–0.28.

The current work is numerical simulation-based research that focuses on the analysis and computer modeling of the biosensor's efficacy against various viruses. Although experimental research is crucial in establishing generalizability and reliability, numerical simulations present an alternative method for comprehending and assessing biosensor performance. They enable us to analyze the behavior of the system in regulated environments, investigate a broad range of scenarios, and evaluate the biosensor's reaction to different virus strains. However, some limitations and potential challenges may be associated with the proposed biosensor in the practical implantations. These factors include environmental conditions, sample preparation, and potential interference from other substances.

Environmental factors that can affect the biosensor's function include humidity, temperature, and electromagnetic noise. Variations in these factors could have an impact on the stability and accuracy of the sensor's readings. However, the implementation of appropriate calibration and temperature compensation techniques is vital in mitigating the impact of environmental elements and guaranteeing dependable outcomes under varying operating conditions. Reliable readings using the biosensor need effective sample preparation. Variability in the results can be introduced by aspects including sample collecting methods, storage environments, and possible degradation of the target analyte. Establishing standardized procedures for sample handling and storage will help to reduce these effects and guarantee reliable measurements. Moreover, the response of the biosensor may be influenced by molecules that interact with the sensing mechanism or compounds that share comparable spectral properties. To improve the biosensor's specificity and reduce the effects of interference, selective coatings or signal processing methods can be used.

This study shows that the proposed sensor, which is insensitive to polarization mode and incident angle up to θ = 90°, can detect viruses without labels, allowing for faster and more accurate identification in different environments. Furthermore, the adjustable structure reduces the requirement for consistent positioning during sample testing, resulting in a more rapid detection process. Experimentally in real-world virus detection applications Terahertz Time-Domain Spectroscopy (THz-TDS) is commonly used [52, 53] and the proposed THz sensor works in tandem with THz-TDS. This integration delivers precise and sensitive information about material properties, molecular structures, and dynamic processes. However, THz-TDS systems are expensive, ranging from tens of thousands to several hundred thousand dollars. This high cost is due to the advanced technology and precision necessary to make, detect, and analyze terahertz waves, yet they are more efficient and faster.

V. CONCLUSION

The analysis and characterization of a metamaterial THz biosensor intended for the detection of different viruses are presented in this work. A flower-shaped resonator is incorporated into the sensor design, and its polarization and angular stability properties are carefully assessed. The results show that the suggested sensor has no decrease in absorptivity and can maintain angular stability of up to 90 degrees without exhibiting polarization sensitivity.

Additionally, the sensor's sensitivity performance is evaluated for several infections. For an M13 bacteriophage with a refractive index of 1.57, the data show a frequency deviation of 524.7 GHz, a peak sensitivity of 920 GHz/RIU, and a figure of merit of 3.8. Furthermore, the effect of sample thickness on sensitivity is examined, resulting in a 350.74 GHz/μm deviance. Overall, the results demonstrate the applicability of the suggested highly sensitive and compact sensor for biological sensing applications, as well as its potential for virus detection and other pertinent uses in the field.

CONFLICT OF INTEREST

All authors have no conflicts of interest.

REFERENCES

1. Cong, L., and Singh, R., “Sensing with THz metamaterial absorbers”. arXiv preprint arXiv:,1408.3711, 2014.
2. M. Nejat and N. Nozhat, "Ultrasensitive THz Refractive Index Sensor Based on a Controllable Perfect MTM Absorber," in IEEE Sensors Journal, vol. 19, no. 22, pp. 10490-10497, 2019.
3. A. Keshavarz and Z. Vafapour, "Sensing Avian Influenza Viruses Using Terahertz Metamaterial Reflector," in IEEE Sensors Journal, vol. 19, no. 13, pp. 5161-5166, 2019.
4. W. Zhang et al., "Ultrasensitive dual-band terahertz sensing with metamaterial perfect absorber," 2017 IEEE MTT-S International Microwave Workshop Series on Advanced Materials and Processes for RF and THz Applications (IMWS-AMP), Pavia, pp. 1-3, 2017.
5. I. Al-Naib, "Biomedical Sensing with Conductively Coupled Terahertz Metamaterial Resonators," in IEEE Journal of Selected Topics in Quantum Electronics, vol. 23, no. 4, pp. 1-5, 2017.
6. P. U. Jepsen, D. G. Cooke, and M. Koch, “Terahertz spectroscopy and imaging—Modern techniques and applications,” Laser Photon. Rev.,vol. 5, no. 1, pp. 124–166, 2011.
7. Watts, C. M., Shrekenhamer, D., Montoya, J., Lipworth, G., Hunt, J., Sleasman, T, Krishna, S., Smith, D.R. and Padilla, W.J, “Terahertz compressive imaging with metamaterial spatial light modulators”, Nature Photonics, vol. 8, no. 8, pp. 605, 2014.
8. V. Sanphuang, W. Yeo, J. L. Volakis and N. K. Nahar, "THz Transparent Metamaterials for Enhanced Spectroscopic and Imaging Measurements," in IEEE Transactions on Terahertz Science and Technology, vol. 5, no. 1, pp. 117-123, 2015.
9. E. MacPherson, G. P. Gallerano, G. -S. Park, H. Hintzsche and G. J.Wilmink, "Guest Editorial: Terahertz imaging and spectroscopy for biology and biomedicine," in IEEE Journal of Biomedical and Health Informatics, vol. 17, no. 4, pp. 765-767, 2013.
10. Z. Wang et al., "Characterization of Thin Metal Films Using Terahertz Spectroscopy," in IEEE Transactions on Terahertz Science and Technology, vol. 8, no. 2, pp. 161-164, 2018.
11. J. M. Jornet and I. F. Akyildiz, “Graphene-based plasmonic nanoantenna for terahertz band communication in nanonetworks,” IEEE J. Sel. Areas Commun., vol. 31, no. 12, pp. 685–694, 2013.
12. H. A. Hafez and M. Elkabbash, "Terahertz sources: A comprehensive review," Optics and Laser Technology, vol. 134, p. 106758, 2021.
13. K. Sakai, "Generation and detection of terahertz waves for biomedical applications," Journal of Infrared, Millimeter, and Terahertz Waves, vol. 39, no. 10, pp. 879-893, 2018.
14. J. Gu, S. Fan, and X. C. Zhang, "Terahertz wave detection: Optics and electronics," in Terahertz Spectroscopy, Springer, 2013, pp. 115-145.
15. S. Foteinopoulou and M. Kafesaki, "Terahertz detectors: A review," Journal of Infrared, Millimeter, and Terahertz Waves, vol. 39, no. 5, pp. 407-439, 2018.
16. Afsaneh Keshavarz, Zohreh Vafapour," Sensing Avian Influenza Viruses Using Terahertz Metamaterial Reflector", IEEE Sensors Journal, vol. 19, issue 13, pp. 5161-5166, Jul. 2019.
17. Dong Cheng,Xia He, Xialian Huang, Bao Zhang,Guo Liu, Guoxiang Shu, Chao Fang, Jianxun Wang, Yong Luo, " Terahertz biosensing metamaterial absorber for virus detection based on spoof surface plasmon polaritons ", Int.J.Rf.Micro.Comput.Aided Eng., vol. 28, issue.7, pp.1-7, Sep. 2018.
18. Areed, Nihal FF, Zienab El-Wasif, and S. S. A. Obayya. "Nearly perfect metamaterial plasmonic absorbers for solar energy applications." Optical and Quantum Electronics 50 (2018): 1-12.
19. Smith, D. R., D. C. Vier, Th Koschny, and C. M. Soukoulis. "Electromagnetic parameter retrieval from inhomogeneous metamaterials." Physical review E 71, no. 3 (2005): 036617.
20. Dogan, E., Emin Unal, Dilek Kapusuz, Muharrem Karaaslan, and C. Sabah. "Microstrip patch antenna covered with left handed metamaterial." Applied Computational Electromagnetics Society Journal 28, no. 10 (2013): 999.
21. J. A. Stewart, T. C. Holland, and A. S. Bhagwat, “Human Herpes Simplex Virus-1 depletes APOBEC3A from nuclei,” Virology, 2019.
22. A. Veeraselvam, G. N. A. Mohammed and K. Savarimuthu, "A Novel Ultra-Miniaturized Highly Sensitive Refractive Index-Based Terahertz Biosensor," in Journal of Lightwave Technology, vol. 39, no. 22, pp. 7281-7287, 15 Nov.15, 2021, doi: 10.1109/JLT.2021.3112529.
23. Aruna Veeraselvam, Gulam Nabi Alsath Mohammed, Kirubaveni Savarimuthu, Radha Sankararajan," A novel multi band biomedical sensor for THz regime", Opt Quant Electron, vol. 53, no.354, pp.1 - 20, 2021.
24. Ma, Anchen, Renbin Zhong, Zhenhua Wu, Yiqing Wang, Long Yang, Zekun Liang, Zheng Fang, and

Shenggang Liu, "Ultrasensitive THz Sensor Based on Centrosymmetric F-Shaped Metamaterial Resonators," Frontiers in Physics, pp. 441, 2020.
25. El-Wasif, Zienab, Tawfik Ismail, and Omnia Hamdy. "Design and optimization of highly sensitive multi-band terahertz metamaterial biosensor for coronaviruses detection." Optical and Quantum Electronics 55.7 (2023): 604.
26. Areed, Nihal FF, Zienab El-Wasif, and S. S. A. Obayya. "Nearly perfect metamaterial plasmonic absorbers for solar energy applications." Optical and Quantum Electronics 50 (2018): 1-12.
27. J. A. Stewart, T. C. Holland, and A. S. Bhagwat, "Human Herpes Simplex Virus-1 depletes APOBEC3A from nuclei," Virology, 2019.
28. C. M. Menendez, and D. J. Carr, "Defining nervous system susceptibility during acute and latent herpes simplex virus-1 infection," Journal of Neuroimmunology, vol. 308, pp. 43-49, 2017.
29. C. M. Kollias, R. B. Huneke, B. Wigdahl, and S. R. Jennings, "Animal models of herpes simplex virus immunity and pathogenesis," Journal of Neurovirology, vol. 21, no. 1, pp. 8-23, 2015.
30. D. M. Knipe, and A. Cliffe, "Chromatin control of herpes simplex virus lytic and latent infection," Nature Reviews Microbiology, 6, no. 3, pp. 211, 2008.
31. A. V. Farooq, and D. Shukla, "Herpes simplex epithelial and stromal keratitis: an epidemiologic update," Survey of Ophthalmology, vol. 57, no.5, pp. 448-462, 2012.
32. J. LeGoff, H.Péré, and L. Bélec, "Diagnosis of genital herpes simplex virus infection in the clinical laboratory," Virology Journal, vol. 11, no.1, pp. 83, 2014.
33. S. Zhang, C. Huo, J. Xiao, T. Fan, S. Zou, P. Qi, L. Sun, M. Wang, and Y. Hu, "p-STAT1 regulates the influenza A virus replication and inflammatory response in vitro and vivo," Virology, 2019.
34. M. Jané, M. J. Vidal, N. Soldevila, A. Romero, A. Martínez, N. Torner, P. Godoy, C. Launes, C. Rius, M. A. Marcos, and A. Dominguez,"Epidemiological and clinical characteristics of children hospitalized due to influenza A and B in the south of Europe, 2010–2016," Scientific Reports, vol. 9, no. 1, pp. 1-7, 2019.
35. T. Shi, Z. Nie, L. Huang, H. Fan, G. Lu, D. Yang, and D. Zhang, "Mortality risk factors in children with severe influenza virus infection admitted to the pediatric intensive care unit," Medicine, vol. 98, no. 35, pp. e16861, 2019.
36. K. W. Hong, H. J. Cheong, J. Y. Song, J. Y. Noh, T. U. Yang, and W. J. Kim, "Clinical manifestations of influenza A and B in children and adults at a tertiary hospital in Korea during the 2011–2012 season," Japanese Journal of Infectious Diseases, vol. 68, no. 1, pp. 20-26, 2015.
37. C. Paules, K. Subbarao, Influenza. Lancet. 12;390, no. 10095, pp. 697-708, 2017.
38. A. Woźniak-Kosek, B. Kempińska-Mirosławska, and G. Hoser,"Detection of the influenza virus yesterday and now," Acta Biochimica Polonica, vol. 61, no. 3, 2014.
39. E. Fanales-Belasio, M. Raimondo, B. Suligoi, and S. Buttò, "HIV virology and pathogenetic mechanisms of infection: a brief overview," Annali dell'Istituto superiore di sanita, vol. 46, pp. 5-14, 2010.
40. B. N. R. Dube, T. P. Marshall, and R. P. Ryan, "Predictors of human immunodeficiency virus (HIV) infection in primary care: a systematic review protocol," Systematic Reviews, vol. 5, no. 1, pp. 158, 2016.
41. UNAIDS. Global HIV AIDS statistics - 2019 fact sheet., 2019.
42. K. C. Abbott, I. Hypolite, P. G. Welch, and L. Y. Agodoa, "Human immunodeficiency virus/acquired immunodeficiency syndrome-associated nephropathy at end-stage renal disease in the United States:patient characteristics and survival in the pre highly active antiretroviral therapy era," Journal of Nephrology, vol. 14, 5, pp. 377-383, 2001.
43. C. A. Agutu, C. J. Ngetsa, M. A. Price, T. F. Rinke de Wit, G. Omosa- Manyonyi, E. J. Sanders, and S. M. Graham, "Systematic review of the performance and clinical utility of point of care HIV-1 RNA testing for diagnosis and care," PloS One, vol. 14, no. 6, pp. e0218369, 2019.
44. C. Weigel, and H. Seitz, "Bacteriophage replication modules," FEMS Microbiology Reviews, vol. 30, no. 3, pp. 321-381, 2006.
45. S. L. Díaz-Muñoz, and B. Koskella, "Bacteria–phage interactions innatural environments," In Advances in Applied Microbiology, vol. 89, pp.
46. 135-183; Academic Press, 2014.
47. L. A. Ogilvie, and B. V. Jones, "The human gut virome: a multifaceted majority," Frontiers in Microbiology, vol. 6, pp. 918, 2015.
48. H. W. Ackermann, "Bacteriophage electron microscopy," In Advances in Virus Research, vol. 82, pp. 1-32; Academic Press, 2012.
49. Z. Vafapour et al., "The potential of refractive index nanobiosensing using a multi-band optically tuned perfect light metamaterial absorber," IEEE Sensors J., vol. 21, no. 12, pp. 13786–13793, Jun. 2022.
50. Z. Zhang et al., "Sensitive detection of cancer cell apoptosis based on the non-bianisotropic metamaterials biosensors in terahertz frequency", Optical Materials Express, vol. 8, no. 3, p. 659, 2018.
51. X. Yan et al., "The terahertz electromagnetically induced transparency like metamaterials for sensitive biosensors in the detection of cancer cells", Biosensors and Bioelectronics, vol. 126, pp. 485-492, 2019.
52. R. Cheng, L. Xu, X. Yu, L. Zou, Y. Shen, and X. Deng, "High sensitivity biosensor for identification of protein based on terahertz Fano resonance metasurfaces", Optics Communications, vol. 473, p.125850, 2020.
53. Shohreh Nourinovin, Akram Alomainy," A Terahertz Electromagnetically Induced Transparency-Like

Metamaterial for Biosensing", IEEE, no.20611732, pp.1-5, 2021.

54. Li, Dongxia, Fangrong Hu, Haipeng Zhang, Zhencheng Chen, Gaoxiang Huang, Fang Tang, Shangjun Lin, Yingchang Zou, and Yuan Zhou, "Identification of Early-Stage Cervical Cancer Tissue Using Metamaterial Terahertz Biosensor With Two Resonant Absorption Frequencies," in IEEE Journal of Selected Topics in Quantum Electronics, vol. 27, no. 4, pp. 1-7, July-Aug. 2021
55. Hou, Xinfu, Xieyu Chen, Tianming Li, Yaoyao Li, Zhen Tian, and Mingwei Wang, "Highly sensitive terahertz metamaterial biosensor for bovine serum albumin (BSA) detection," Optical Materials Express, vol. 11, no. 7, pp. 2268-2277, 2021.